GEOLOGICAL SURVEY OF CANADA
COMMISSION GEOLOGIQUE DU CANADA
OPEN FILE 2187

MASS TRANSFER OF ELEMENTS IN MIDDLE TRIASSIC SHALE/SANDSTONE SEQUENCES, SVERDRUP BASIN, ARCTIC ISLANDS

PART 2: MINERALOGY, CLAY MINERALOGY, THERMOGRAVIMETRIC ANALYSIS AND CHEMISTRY OF THE >.2μ m FRACTION AND SEM STUDIES ON THIN SECTIONS, EAST DRAKE L-06 AND SKY BATTLE BAY M-11 CORES

by

Anthony E. Foscolos

Geochemist/Mineralogist
School of Mineral Resources Engineering
Technical University of Crete
Chania 73132, Crete
Greece

and

Geological Survey of Canada
Institute of Sedimentary and Petroleum Geology
3303 - 33rd Street N.W.
Calgary, Alberta T2L 2A7
Canada

December, 1989

TABLE OF CONTENTS

*Note: Appendix II is not included in the open file report, but can be viewed at the Geological Survey of Canada Library, Institute of Sedimentary and Petroleum Geology, 3303-33rd St. N.W., Calgary, Alberta.

LIST OF FIGURES

Figure 10. X-ray diffraction patterns of Ca-saturated <.2μm fraction from Skybattle Bay M-11 well samples, at 50 per cent R.H.; (a) Calcareous laminated shale at 2520.51 m; (b) Calcareous laminated shale at 2520.95 m; (c) Bone bed (major unconformity) at 2531.34 m; (d) Bone bed (major unconformity) at 2531.48 m; (e) Bioturbated calcareous sandstone at 2531.53 m; (f) Bioturbated calcareous sandstone from 2531.84 m; (g) Transition zone at 2532.02 m; (h) Calcareous silty shale at 2533.50 m.

LIST OF TABLES

INTRODUCTION

This research is a continuation of a previous study carried out by Foscolos et al. (1988) and concerns the influence of diagenesis and catagenesis on the chemistry and mineralogy of the fine fraction encountered in shales and adjacent sandstones.

Diagenetic transformations are detected much more readily in fine fractions than by whole rock analysis (Foscolos and Kodama 1974; Foscolos et al., 1976; Foscolos and Powell, 1979). Therefore, to identify mineralogical and chemical changes from shale, to the shale/sandstone interface, to sandstone, the very fine clay fraction has to be isolated and studied in detail.

The research reported herein was complicated because shales and sandstones from the two wells studied, East Drake L-06 and Skybattle Bay M-11, are rich in carbonate minerals. Thus, the isolation of <.2 μm clay fraction from the previously isolated <2 μm clay fraction of the calcareous shales, limestones and calcareous sandstones was tedious. After removal of calcite and dolomite from the clay-sized faction, the carbonate free <.2 μm fraction was isolated by ultracentrifugation. Discrete minerals and interstratified layer silicates from this fraction were studied in detail by X-ray diffraction. Furthermore, thermogravimetric analyses (T.G.A.) and chemical analyses were carried out. The aim of T.G.A. was to measure changes of absorbed H_2O, cavity H_2O, and crystal lattice H_2O in order to quantify minerals and assign absorbed water which is related to the type of 2:1 interstratified layer silicates.

Effort was also undertaken to study clay minerals in pore throats by Scanning Electron Microscopy (S.E.M.) on thin sections.

Acknowledgments

The author wishes to thank Messrs A.G. Heinrich, B.L. Gorham and Mrs. J. Wong for their technical assistance. Drs. R.W. Macqueen and H. Abercrombie kindly revised a draft manuscript of this open file report.

MATERIALS AND METHODS

X-Ray diffraction of the <.2 μm fraction

Fifty-one carbonate free <.2 μm size fraction samples were prepared from calcareous shales, limestones, and calcareous sandstones from the core of East Drake L-06 well. Similarly, forty-four <.2 μm fractions were obtained from core of the Skybattle Bay M-11 well (Figs. 1 and 2). The geologic and stratigraphic setting of these cores and a brief description is given by Embry and Podruski (1988).

To acquire the <.2 μm fraction, the <2 μm fraction was suspended in H_2O and centrifuged for 24.58 minutes (Appendix I). The supernatant liquid containing the <.2 μm fraction was subsequently divided into two equal portions. One portion was saturated with a monovalent cation, potassium, and the other portion with a divalent cation, calcium. Excess cations were removed by five washings with distilled water and subsequent centrifugations. Finally the samples were recovered by freeze-drying.

X-ray analyses (Brydon et al., 1963) on oriented specimens were initially carried out on one hundred and ninety (190) samples. Ninety five samples were saturated with Ca and ninety-five were saturated with K. Specimen orientation was achieved by delivering 0.5 ml clay suspension containing 20 mg of sample to a 19 x 12.5 mm glass slide. After drying, the samples were analyzed using Fe filtered Co Kα, radiation (λ = 1.7902Å) with settings 40 KV-20m A, scanning speed 1° (2θ) min^{-1}, and a time constant of 2 seconds.

From the original 190 <.2 μm fractions, sixty-two (62) fractions obtained from different lithologies from both wells, East Drake L-06 and Skybattle Bay M-11, were selected for further X-ray investigation under various treatments such as absence of humidity, glyceration to maximize expansion of smectitic components, and heat treatment at 550°C. Using samples obtained by these treatments, silicates, hydrous silicates, 2:1 interstratified layer silicates, and other minerals were studied on the basis of criteria used by Kodama and Brydon (1968). In all, three hundred and sixty-eight diffraction patterns were studied.

Thermal analysis of the Ca saturated <.2 μm fraction

Thermogravimetric analysis (T.G.A.) was carried out on Ca-saturated air-dried samples and on samples heated to 550°C for 2.5 hours. The aim was to use crystal lattice water content of the layer silicates as a measure of their concentration, following Barshad (1965). Once the clay minerals are quantified, the absorbed water of the interstratified 2:1 layer silicates can also be evaluated. The latter is a measure of the expandable clays and therefore can be used to assess minute transformation of the 2:1 interstratified layer silicates in shale and sandstone sequences. This method of quantification of clay minerals was used by Foscolos and Kodama (1974) to evaluate kaolinite concentration in <.08 μm fractions.

For T.G.A. measurements, 10 mg of sample were transferred to a Perkin-Elmer T.G.S.-2 apparatus. Analyses were carried out at a constant heating rate of 80°C/min from ambient to 1000°C, and losses at 150°C, 370°C, and 1000°C were reported. In this work, the results from 62 samples are reported.

Chemical analysis

Elemental analysis of Ca-saturated air dried samples was carried out by fusing 100 mg of sample with $LiCO_3$ and H_3BO_3. Elemental concentrations were determined using the method of Foscolos and Barefoot (1970).

Scanning Electron Microscopy (S.E.M.)

S.E.M. analysis was carried out on thin sections to identify and study the texture of clays in pore throats. Coverless thin sections were carbon coated to ensure good surface conductivity. The study was carried out using a Cambridge Stereoscan 150MK2 with a KEVEX 7000 energy dispersive X-ray analysis (EDX) system.

RESULTS

X-ray diffraction of the <.2 μm fraction

Semiquantitative analysis of the <.2 μm fraction from the East Drake L-06 well reveals the presence of illite, kaolinite, interstratified 2:1 layer silicates, and quartz in almost all samples (Table 1). Feldspars are encountered at 1128.91-1129.93 m and 1132.65-1132.67 m. In previous work by Foscolos et al. (1988), the presence of clays was not obvious owing to the abundance of carbonates.

Quartz is ubiquitous in all <.2 μm fractions, but it is more abundant in the <.2 μm fraction of sandstones than in shales. Kaolinite is absent from both shales and sandstones in the interval between 1122.86 and 1130.95 m, that is for 8.09 m. Below this depth, kaolinite concentration increases substantially, being more or less equal to the illite concentration between 1130.26 and 1141.90 m (that is for 11.76 m). The lithology of this interval is dominated by argillaceous siltstones, brown calcareous shales, and glauconitic sandstones. From 1143.73 to 1157.44 m illite concentration equals kaolinite. However, the latter mineral is not as well crystallized as in the previous section. The d_{001} and d_{002} spacings at 7.16 Å and 3.57 Å are represented by broad peaks, indicating either incipient formation of kaolinite or its destruction.

The 2:1 interstratified layer silicates are of special interest in this study because they exhibit different patterns depending on the distance from the shale/sandstone interface. At the shale/sandstone interface, 1125.12-1125.15 m, the expandable component disappears and a well crystallized 2:1 layer silicate, illite, is predominant (Fig. 3). As one moves upward into shale, the expandable component starts to appear as a tail, for example at 1123.38-1123.40 metres depth, whereas in the uppermost sample examined, 1122.68 to 1122.79 m, a shoulder begins at 14 Å and remains to 10.0 Å. The X-ray diffractograms (Fig. 7) show that the 001 basal reflection peak widens at its base from 10.2Å at 0 per cent relative humidity (R.H.) to 12 Å at 50 per cent R.H. to 14 Å with glycerol. Upon glycerolation a plateau is formed between 14 Å and 12 Å. The widening of the 001 basal reflections decrease as the shale/sandstone interface is approached, disappearing completely at the shale/sandstone interface (depth 1125.12-1125.15 m). Below the shale/sandstone interface, that is within the sandstone unit, the 001 basal reflection at 50 per cent R.H. wideness forming a plateau

from 16 Å to 10 Å (Fig. 3). Unlike the clays form the shale unit, the width of this plateau stays the same to 1132.74 m (Fig. 3). This implies that the concentration of the expandable component in the intrstratified 2:1 layer silicates is always the same starting from the shale/sandstone interface to the depth of 1132.74 m.

The existence of an expandable component within the interstratified layer silicates of the shale unit, which decreases in concentration as the shale/sandstone interface is approached, and increases in the sandstone unit has been

observed at three other intervals within the studied core interval of the East-Drake L-06 well. These intervals are from 1131.89 to 1137.49 m (Fig. 4); from 1137.82 to 1147.56 m (Fig. 5); and from 1149.57 to 1154.40 m (Fig. 6). Worth noticing is also the concentration of the expandable component within the interstratified layer silicates of the sandstone. This concentation is constant regardless of the depth of the sandstone unit (1125.12 m - 1132.74 m, Fig. 3).

The type of expandable components in the <.2 μm fraction of shales was determined in order to compare them with the type of expandable components encountered in the same fraction in the sandstones. To achieve this, X-ray diffractograms were obtained with various absorbed cations, Ca^{2+} and K^{+}, various conditions of relative humidity (R.H.), glyceration, that is adding organic molecules in the interlayer spacing to maximize expansion, and heating at 550°C for 2.5 hours in order to destroy kaolinite and emphasize the presence of chlorite or chlorite-like components. Thus, a <.2 μm fraction isolated from a shale, 1122.76-1122.79 metres depth, shows that the first order basal reflection from 10.2 Å at 0% R.H. gradually widens at 50% R.H., yielding its maximum expansion upon glyceration (Fig. 6). This maximum expansion is exhibited as a shoulder starting from 14 Å to 10 Å. Upon heating to 550°C the expansion disappears totally. This continuous expansion indicates the presence of a smectite-like component in conjunction with a mica-like component. The K-saturated sample, upon receiving the same treatment, yields a limited expansion (Fig. 7). This behaviour indicates that, in addition to the smectitic component, a vermiculite-like component also exists in the interstratified layer silicates. If only one expandable 2:1 layer silicate existed in the 2:1 interstratified layer silicates, that is smectite <u>or</u> vermiculite, then, under the same conditions, similar

diffractograms should have been obtained regardless of the interlayer cation (Kodama and Brydon, 1968). No discrete expandable minerals were present in the <.2 μm fractions since no peaks were observed at ~15 Å (vermiculite) and ~16 Å (smectite) in the diffractograms of the Ca saturated fractions at 50% R.H. The absence of these peaks and the behaviour of the clays under the various conditions outlined above indicate that illite, smectite and vermiculite exist as component layers in the 2:1 interstratified, hydrous layer silicates.

X-ray diffraction patterns of the oriented <.2 μm fraction near the shale/sandstone interface, at 1125.12-1125.15 m, indicate that regardless of the absorbed ion, Ca^{2+} or K^{+}, and regardless of the treatment, only one hydrous layer silicate exists, that is discrete illite (Fig. 8). The difference in x-ray patterns of the <.2 μm fractions between the two depths is obvious when Figure 7 is compared with Figure 8.

X-ray diffraction patterns of an oriented <.2 μm specimen from a sandstone, 1128.91-1128.93 m, again shows the presence of expandable 2:1 layer silicates (Fig. 9). However, by studying the shape of the diffractogram of expandable components and the lack of complete collapse of the interstratified layer silicates upon heating to 550°C for 2.5 hours, it is speculated that a pseudoquaternary system of smectite - vermiculite - chlorite -illite is formed. This is deduced from two lines of evidence, the lack of good crystallization at 10 Å and the absense of the d_{002} and d_{020} peaks at 5 Å and 4.4 Å respectively. Both peaks appear upon heating to 550°C, regardless of the ion absorbed on the clay surface (Fig. 9).

Semiquantitative mineralogical analysis of the <.2 μm fraction from the Skybattle Bay M-11 core reveals two distinct groups of minerals. The first group consists of quartz, illite and interstratified layer silicates, while the second group contains quartz and interstratified layer silicates (Table 2). The first group of mineral is encountered in two portions of the cored well. The first portion lies between 2520.51 and 2527.79 metres depth and the second portion lies between 2531.38 to 2536.35 metres depth. Between these two segments there is an interval of 4.97 metres, 2531.38 to 2536.35 metres depth, were illite is absent. Worth noting is the absence of kaolinite mineral from the <.2 μm fraction throughout the studied well core.

Interstratified layer silicates in the <.2 μm fraction seems to decrease as one approaches the transition zone between calcareous silty shale or mudstone and the bone bed (Fig. 10). Though not obvious as in the studied cores of the Ca-saturated <.2 μm fraction from East Drake L-06 (Fig. 3), interstratification of 2:1 layer silicates decreases as the boundary between shales and bone bed is approached.

Thermogravimetric analysis of the Ca-saturated <.2μm fraction

T.G.A. was used to study the dehydration pattern of the 2:1 interstratified layer silicates. For this purpose one set of samples was run without any treatment (Table 3), while the second set was run after heating sample to 550°C for 2 1/2 hours (Table 4). The latter treatment destroys kaolinite while leaving the 2:1 interstratified layer silicates almost intact. As a result, since the only minerals containing volatile components are the 2:1 hydrous layer silicates, then the per cent crystal lattice water of these minerals, as measured by thermogravimetric analyis, is used to better quantify their presence in the <.2μm fraction (Barshad, 1965).

Using published data of absorbed and crystal-lattice water of clay minerals as well as temperatures at completion of desorption and at the start and completion of dehydration (Table 5), the <.2μm fraction of one interval of the East Drake L-06 well was studied. This interval was selected due to the lack of kaolinite in most specimens (Table 1). The results are summarized in Table 6 and indicate that H_2O is "sloughing off" at the shale/sandstone interface, at 1124.53 - 1124.55 m. Above this interface, that is in the shale (1123.38-1123.40 m), absorbed and cavity H_2O reaches 9.2 per cent whereas in the sandstone immediately below the shale/sandstone interface (1125.92 - 1125.95 m), absorbed and cavity water reaches 8.5 per cent.

Data from the Skybattle Bay M-11 well show high crystal lattice H_2O contents (Table 3). On ignition basis crystal lattice water, that is H_2O^+, measured between temperatures of 370°C to 1000°C, is over 5.0 per cent. Based on published data (Barshad, 1965) vermiculite is the only clay mineral with layer water desorption over 370°C (Table 5). Therefore, to measure crystal lattice H_2O^+ over 5.0 per cent on ignition basis implies that in the 2:1 interstratified layers a vermiculite-like component

exists in both shales and sandstones. This is also concluded from the X-ray work of the <.2 μm fraction.

Clay chemistry of the Ca saturated <.2 μm fraction

Analytical results of elemental analysis of the Ca-saturated <.2 μm fraction are presented in Table 7. The aim of this analysis was to relate X-ray work on the dehydration of the clays to their potassium concentration. It has been shown by Foscolos et al. (1976) and Powell et al. (1978) that as potassium concentration increases on the adsorbed sites of the 2:1 layer silicates, adsorbed H_2O decreases. In the interval between 1122.68 and 1125.95 metres depth, East Drake L-06 well, K_2O content in the 2:1 layer silicates increases as the shale/sandstone interface is approached (Table 8).

If kaolinite, quartz, and amorphous silica, aluminum and iron were measured following differential dissolution methods (Jackson, 1965), better results could have been obtained. These techniques, however, were not pursued due to lack of sample. The amount of clay allocated for chemical analysis, in most cases, did not exceed 100 mg, because clay concentrates were very hard to collect from calcareous shales, limestones and calcareous sandstones.

S.E.M. studies on clays in thin sections

An attempt was made to study the shape of the clay layer silicates by S.E.M., to examine their location in pore throats and evaluate their chemical composition. The results were not rewarding and, although S.E.M. photomicrographs are attached to this report as part of this work (Appendix II), they did not assist in the study of the mass transfer of elements from calcareous shales to limestones and calcareous sandstones.

DISCUSSION

The results of this study show that diagenetic changes, especially in hydrous layer silicates, take place within thin sedimentary interval of a few metres in thickness, provided a drainage system is present to accept the byproducts of the reactions.

X-ray results on the fine fractions show a d_{001} peak movement of the hydrous 2:1 interstratified layer silicates upon descending from the shale to the shale/sandstone interface, to the sandstone (Fig. 3). The expanded d_{001} spacing of the 2:1 layer silicates collapses as the shale/sandstone interface is approached. This implies that adsorbed H_2O is sloughing off. Finally, water is reabsorbed on the layer silicates as deduced from the broadening of the d_{001} peak from 10Å-14Å in the sandstone. The X-ray data are substantiated by thermogravimetric analyses. The reason for the transformations observed by XRD and TGA analysis are attributed to the elemental changes which have occurred within the crystal lattices of the layer silicates. This implies that elements have been transferred in order to reconstruct new hydrous layer silicates or, to transform existing 2:1 layer silicates by isomorphic substitution. Identical changes have been studied extensively by Foscolos and Kodama (1974) and Foscolos et al. (1976). Changes in the unit cell of interstratified 2:1 layer silicates due to diagenesis are fingerprinted by the migration of d_{001} spacings. Water loss from adsorbed 2:1 interstratified layer silicates is accompanied by isomorphic substitution of silica by aluminum ions in the tetrahedral layers. To counterbalance the loss of charge, potassium, with valence of +1, is absorbed irreversibly on the clay surfaces causing the expandable clays to become non-expandable. Thus illitization takes palce. This process has been observed by X-ray diffraction at three different levels within the cores studied from the East Drake L-06 well (Figs. 3, 4, 5) and one level in the Skybattle M-11 well core (Fig. 10).

In the interval between 1122.68 and 1130.25 metres depth, East Drake L-06 well, K_2O concentrations of the 2:1 layer silicates increase as the shale/sandstone boundary is approached (Table 8). By comparing X-ray diffractograms (Fig. 10) with K_2O results (Table 8) it is observed that the stepwise changes in chemical composition of the 2:1 interstratified layer silicates may also be detected by X-ray analysis. Although it is very difficult to quantify the movement of elements within the interval between 1122.68 and 1125.12 metres depth due to lack of samples, the fact that stepwise changes in the d_{001} spacing of layer silicates has been recorded, which reflects changes in the structure of clays, implies that transfer and exchange of elements such as silica, aluminum, potassium and calcium took place from 1122.68 to 1125.12 metres depth. Silica had to move out of the

2:1 layer silicate minerals in order for it to be replaced by aluminum. Moreover, calcium had to be displaced by potassium on the clay surfaces in order for H_2O to be "sloughed off". This pattern is repeated at three different levels within the studied core from East Drake L-06 well, namely 1131.89 to 1136.70 metres depth (Fig. 4), 1137.82 to 1144.10 metres depth (Fig. 5) and 1149.57 to 1151.63 metres depth. Moreover, the same pattern is also observed in one level of the Skybattle Bay M-11 well core, namely between 2520.51 and 2531.34 metres depth.

Although the present work did not address the quantitative aspect of the mass transfer of elements, the stepwise and sequential transformation of 2:1 layer silicates in the <.2μm fraction, which is observed repeatedly within the studied core, is most easily explained by the element being mobilized from dissolved minerals. The latter has been noted by Perry and Hower (1970 and 1972).

CONCLUSIONS

Diagenetic changes in fine mineral fractions have been observed by X-ray diffraction, thermal, and chemical analysis within short shale intervals and depend upon the occurrence of a drainage system adjacent to the shales, such as sandstone or bone bed. Quantitative aspects of these changes were not evaluated owing to lack of sufficient samples from both shales and sandstones. Adequate sample size would have enabled us to proceed with detailed chemical work, such as differential dissolution techniques, in order to quantify quartz and various feldspars, and amorphous (non-crystalline) material which is difficult to detect and quantify by XRD.

Because the cores studied contained abundant detrital carbonates, additional work could be carried out to determine the mineralogy, petrology, and diagenetic history of the carbonates. This would involve microscopic and SEM examination to determine the possible effects of dolomitization or mineral dissolution in creating secondary porosity. Additional major and trace element analyses and isotopic analyses may shed light on the type of fluids involved in cementation and diagenesis. Studies of fission tracks in detrital apatites and fluid inclusions in cements may help understand the thermal evolution of these sediments and the Sverdrup Basin in general.

Together, these data will help answer questions related to the provenance, sedimentary environments, diagenesis, thermal history and petroleum potential of these rocks. Additional sampling will be required to carry out this work.

BIBLIOGRAPHY

Barshad, I.
1965: Thermal analysis techniques for mineral identification and mineralogical composition; in Methods of Soil Analysis, C.A. Black (ed.), Part 1, p. 699-742.

Brydon, J.E., Rice, H.M., and Scott, G.C.
1963: The recovery of clays from suspension by freeze-drying; Canadian Journal of Soil Science, v. 43, p. 404-405.

Embry, A.F. and Podruski, J.A.
1988: Third-order depositional sequences of the Mesozoic succession of Sverdrup Basin; in Sequences, Stratigraphy, Sedimentology: Surface and Subsurface; Canadian Society of Petroleum Geologists, Memoir 15, p. 73-83.

Foscolos, A.E. and Barefoot, R.R.
1970: A buffering and standard addition technique as an aid in the comprehensive analysis of silicates by atomic absorption spectroscopy; Geological Survey of Canada, Paper 70-16.

Foscolos, A.E. and Kodama, H.
1974: Diagenesis of clay minerals from Lower Cretaceous shales of northeastern British Columbia; Clay and Clay Minerals, v. 22, p. 319-335.

Foscolos, A.E. and Powell, T.G.
1979: Catagenesis in shales and occurrence of authigenic clays in sandstones, North Sabine H-49 well, Canadian Arctic Islands; Canadian Journal of Earth Science, v. 16, p. 1309-1314.

Foscolos, A.E. and Powell, T.G.
1980: Mineralogical and geochemical transformation of clays during burial catagenesis and their relation to oil generation; Canadian Society of Petroleum Geologists, Memoir 6, p. 153-172.

Foscolos, A.E., Embry, A.F., Snowdon, L.R., and Podruski, J.A.
1988: Mass transfer of elements in Middle Triassic shale/sandstone sequences, Sverdrup Basin, Arctic Islands. Part 1: Mineralogy, composition, SEM character and Rock-Eval/TOC results, East Drake L-06 and Skybattle Bay M-11 cores; Geological Survey of Canada, Open File Report 1812.

Foscolos, A.E., Powell, T.G., and Gunther, P.R.
1976: The use of clay minerals, inorganic and organic geochemical indicators for evaluating the degree of diagenesis and oil generating potential of shales; Geochimica et Cosmochimica Acta, v. 40, p. 953-960.

Kodama, H. and Brydon, J.E.
1968: A study of clay minerals in podzol soils in New Brunswick, Eastern Canada; Clay Minerals, Bulletin 7, p. 295-309.

Perry, E. and Hower, J.
1970: Burial diagenesis in Gulf Coast pelitic sediments; Clay and Clay Minerals, v. 18, p. 165-177.

1972: Late stage dehydration in deeply buried pelitic sediments; American Association of Petroleum Geologists, Bulletin 56, p. 2013-2021.

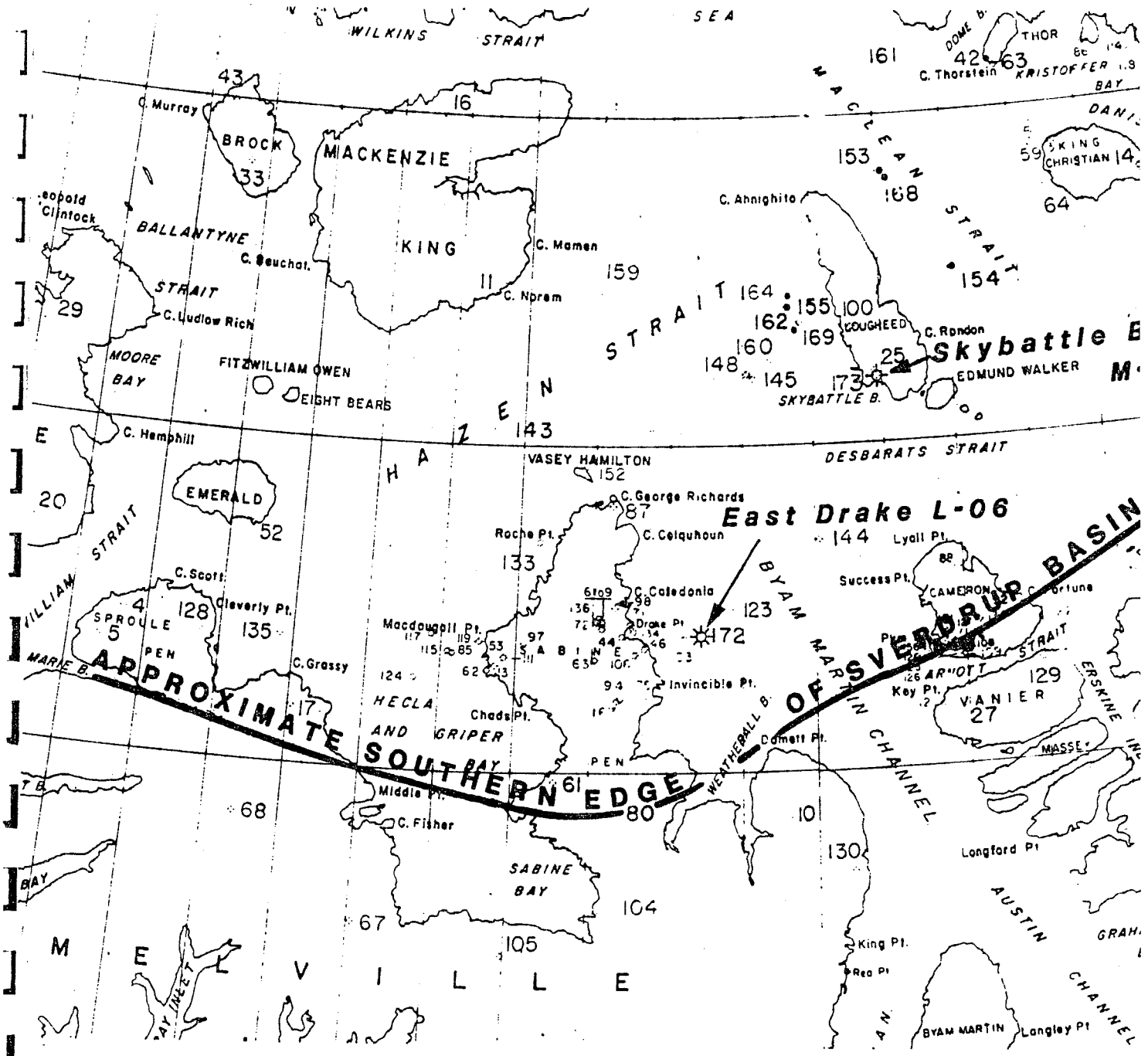

igure 1. Location map, southwestern Sverdrup Basin, Arctic Islanc

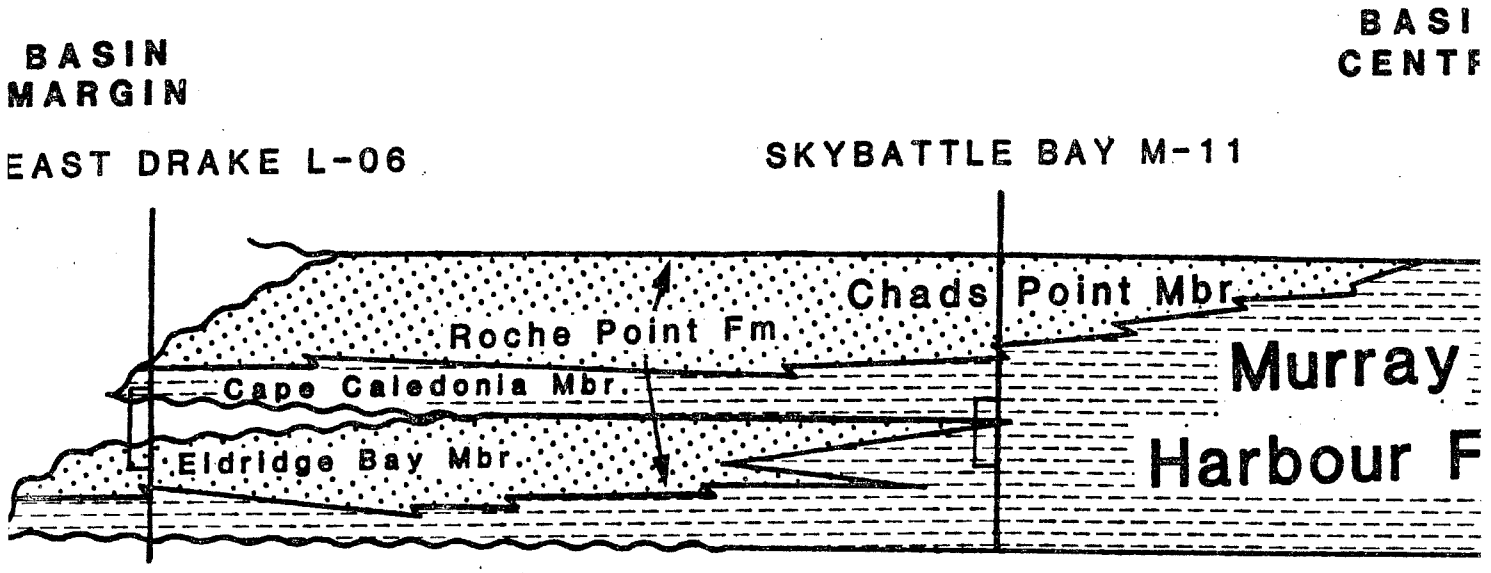

Figure 2. Schematic section, Middle Triassic stratigraphy, western Sverdrup Basin. Cored intervals shown.

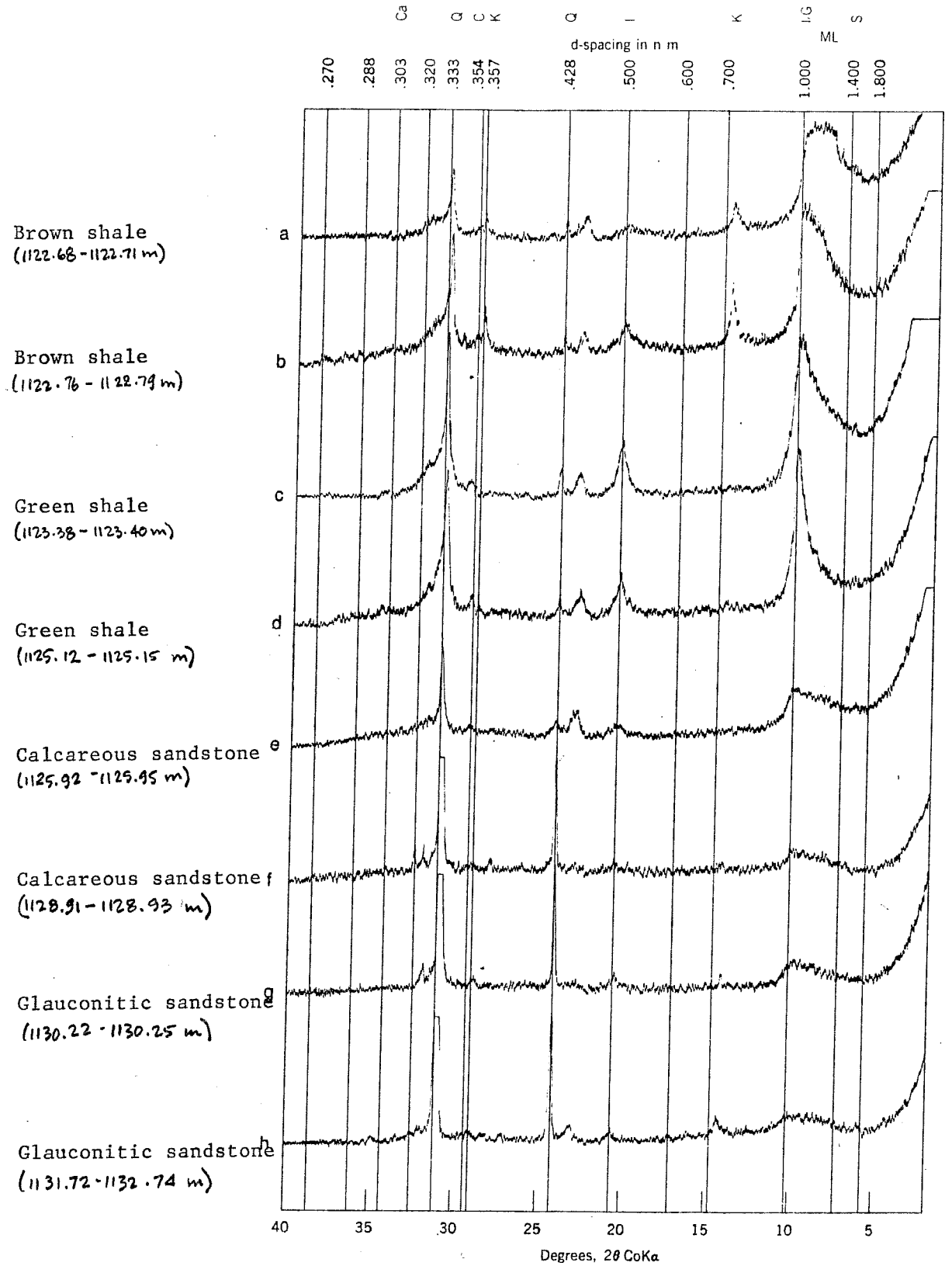

Figure 3. X-ray diffraction patterns of Ca-saturated, <.2μm fraction from East Drake L-06 well samples, at 50 per cent R.H. (a) Brown shale from 1122.68-1122.71 metres depth; (b) Brown shale from 1122.76-1122.79 metres depth; (c) Green shale from 1123.38-1123.40 metres depth; (d) Green shale from 1125.12-1125.15 metres depth; (e) Calcareous sandstone from 1125.92- 1125.95 metres depth; (f) Calcareous sandstone from 1128.91-1128.93 metres depth; (g) Glauconitic sandstone from 1130.22-1130.25 metres depth; (h) Glauconitic sandstone from 1131.72-1132.74 metres depth.

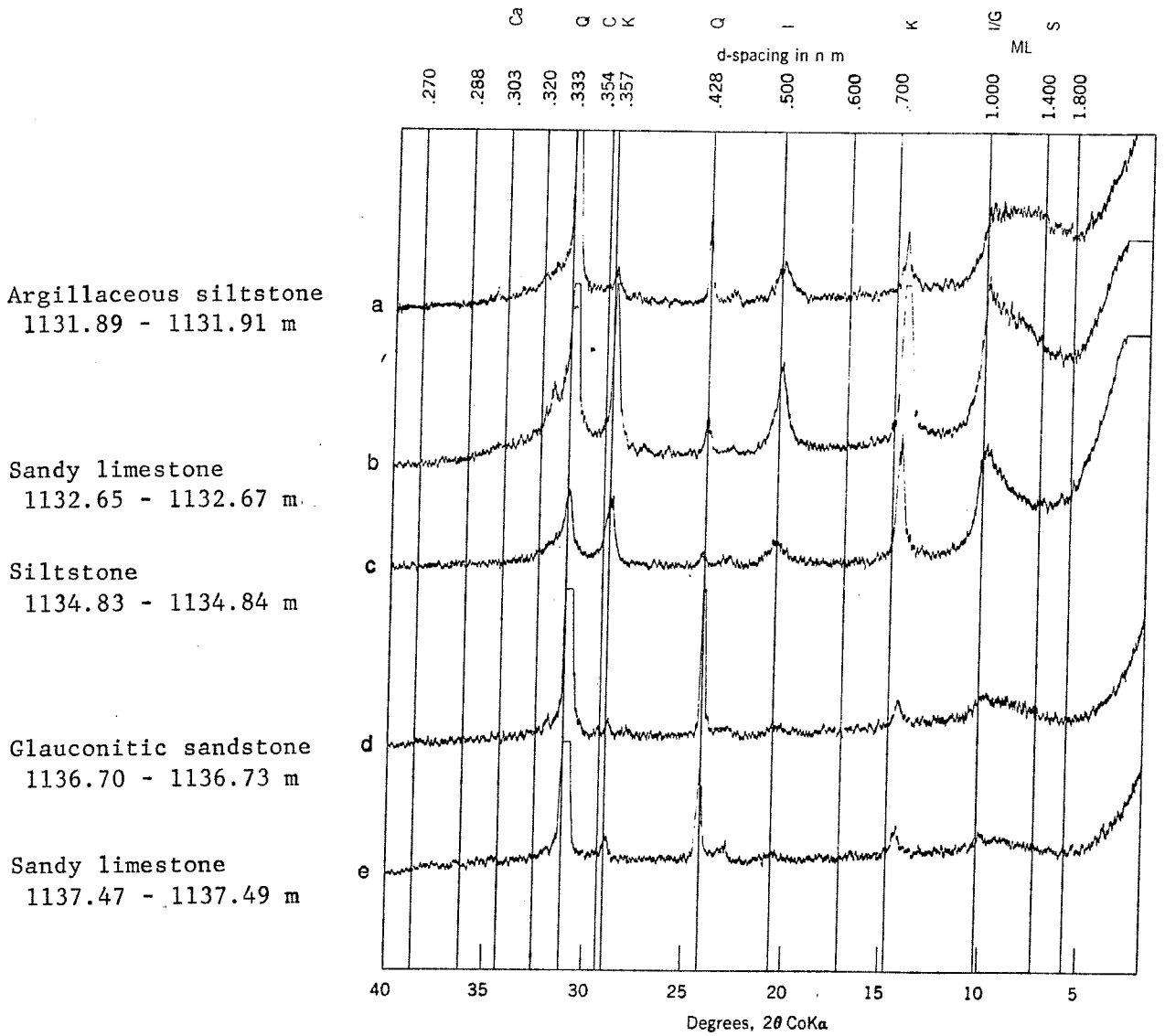

Figure 4. X-ray diffraction patterns of Ca-saturated, <.2μm fraction from East Drake L-06 well samples, at 50 per cent R.H. (a) Argillaceous siltstone from 1131.89-1131.91 metres depth; (b) Sandy limestone from 1132.65-1132.67 metres depth; (c) siltstone from 1134.83-1134.84 metres depth; (d) Glauconitic sandstone from 1136.70-1136.73 metres depth; (e) Sandy limestone from 1137.47-1137.49 metres depth.

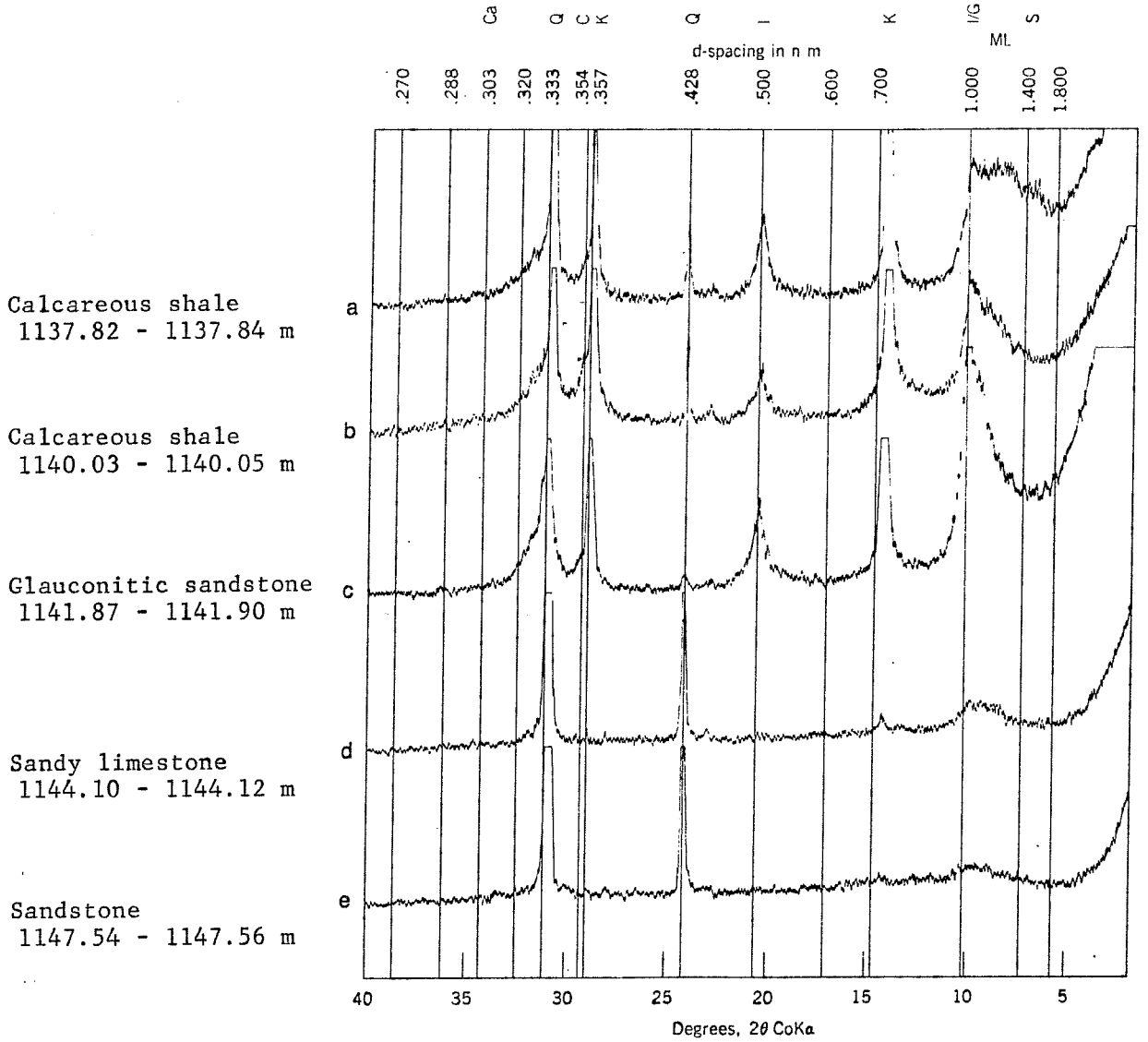

Figure 5. X-ray diffraction patterns of Ca-saturated, <.2μm fraction from East Drake L-06 well samples, at 50 per cent R.H. (a) Brown calcareous shale from 1137.82-1137.84 metres depth; (b) Brown calcareous shale from 1140.03- 1140.05 metres depth; (c) Glauconitic sandstone from 1141.87-1141.90 metres depth; (d) Sandy limestone from 1144.10-1144.12 metres depth; (e) Sandstone from 1147.54-1147.56 metres depth.

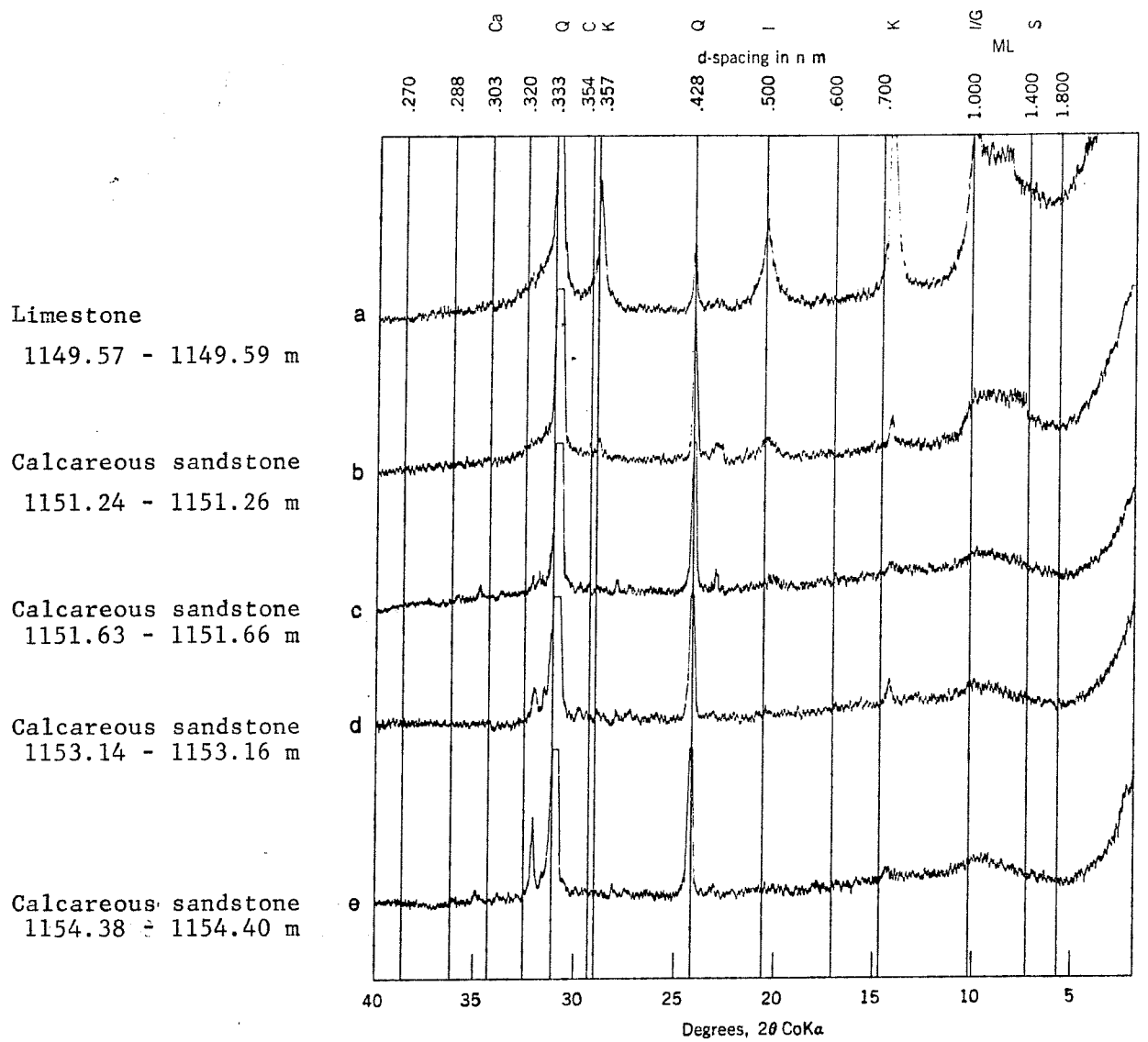

Figure 6. X-ray diffraction patterns of Ca-saturated, <.2μm fraction from East Drake L-06 well samples, at 50 per cent R.H. (a) Limestone from 1149.57- 1149.59 metres depth; (b) Calcareous sandstone from 1151.24-1151.26 metres depth; (c) Calcareous sandstone from 1151.63-1151.66 metres depth; (d) Calcareous sandstone from 1153.14-1153.16 metres depth; (e) Calcareous sandstone from 1154.38-1154.40 metres depth.

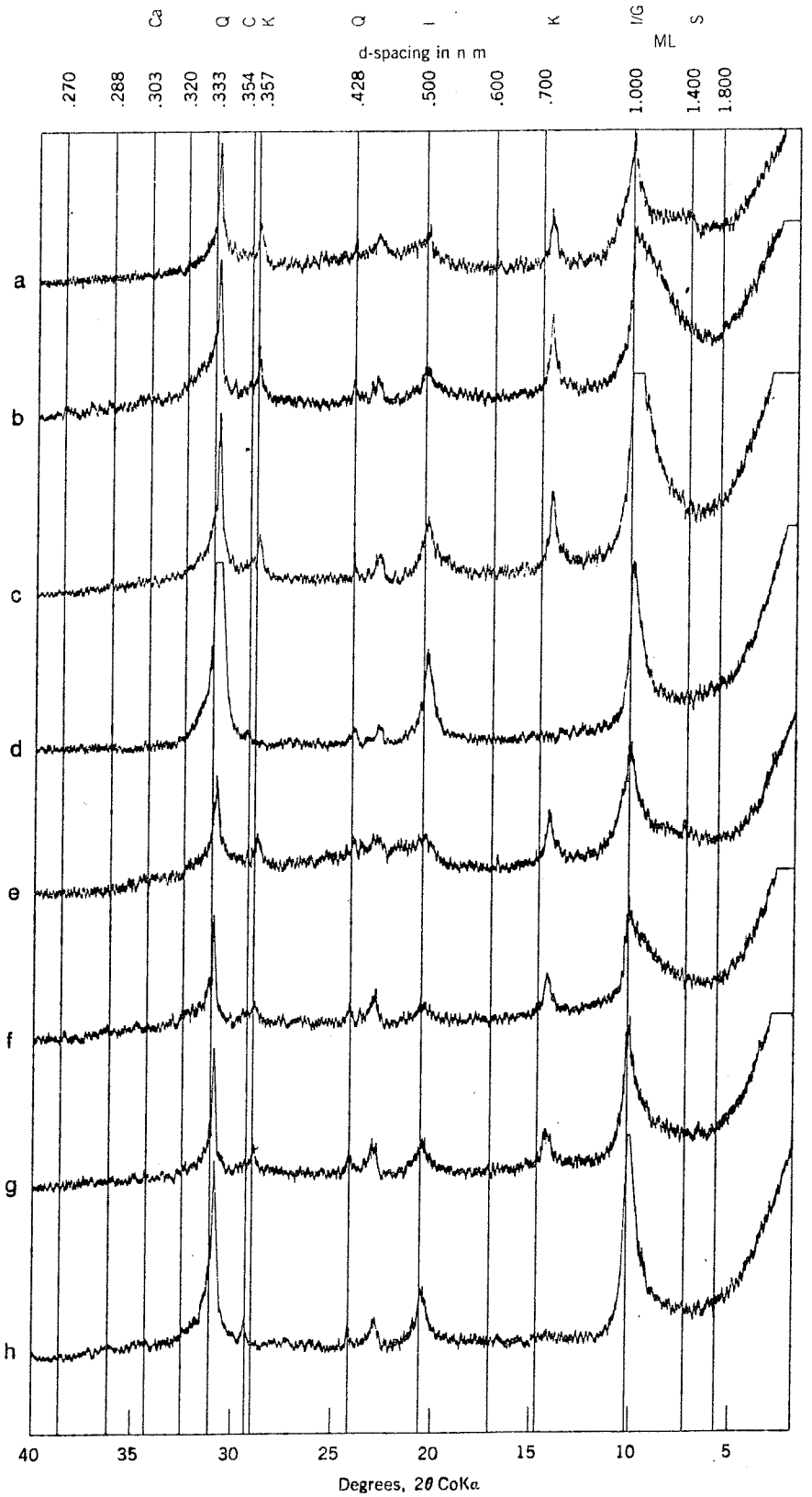

Figure 7. X-ray diffraction patterns of the <.2μm fraction from a brown shale, East Drake L-06 well, 1122.76-1122.79 metres depth; (a) Ca-saturated, glycerol-treated specimen; (b) Ca-saturated specimen at 50 per cent R.H.; (c) Ca-saturated specimen at 0 per cent R.H.; (d) Ca-saturated specimen after heating at 550°C; (e) K-saturated, glycerol-treated specimen; (f) K-saturated specimen at 50 per cent R.H.; (g) K-saturated specimen at 0 per cent R.H.; (h) K-saturated specimen after heating at 550°C.

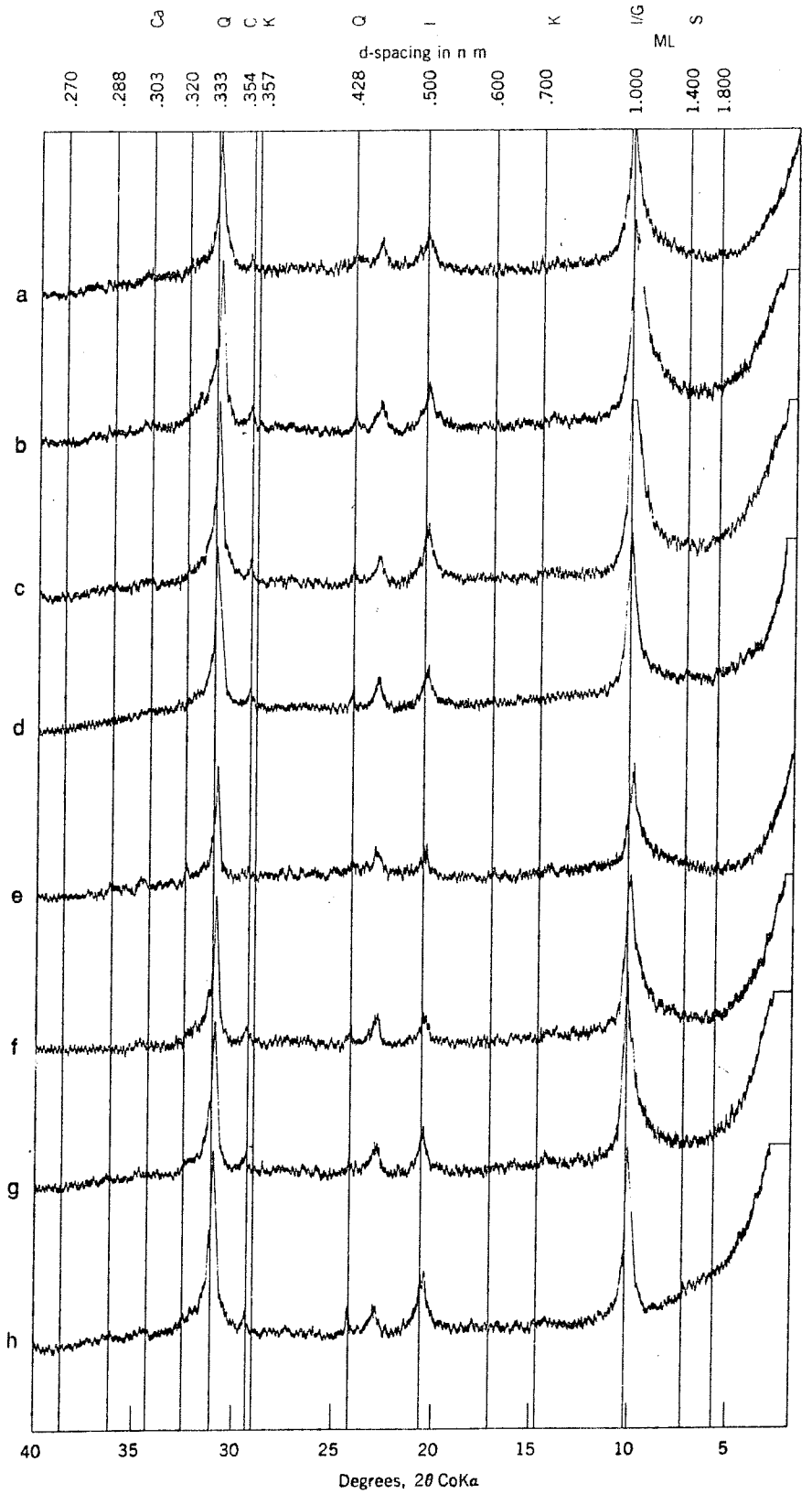

Figure 8. X-ray diffraction patterns of the <.2μm fraction from a green shale, East Drake L-06 well, 1125.12-1125.15 metres depth; (a) Ca-saturated, glycerol-treated specimen; (b) Ca-saturated specimen at 50 per cent R.H.; (c) Ca-saturated specimen at 0 per cent R.H.; (d) Ca-saturated specimen after heating at 550°C; (e) K-saturated, glycerol-treated specimen; (f) K-saturated specimen at 50 per cent R.H.; (g) K-saturated specimen at 0 per cent R.H.; (h) K-saturated specimen after heating at 550°C.

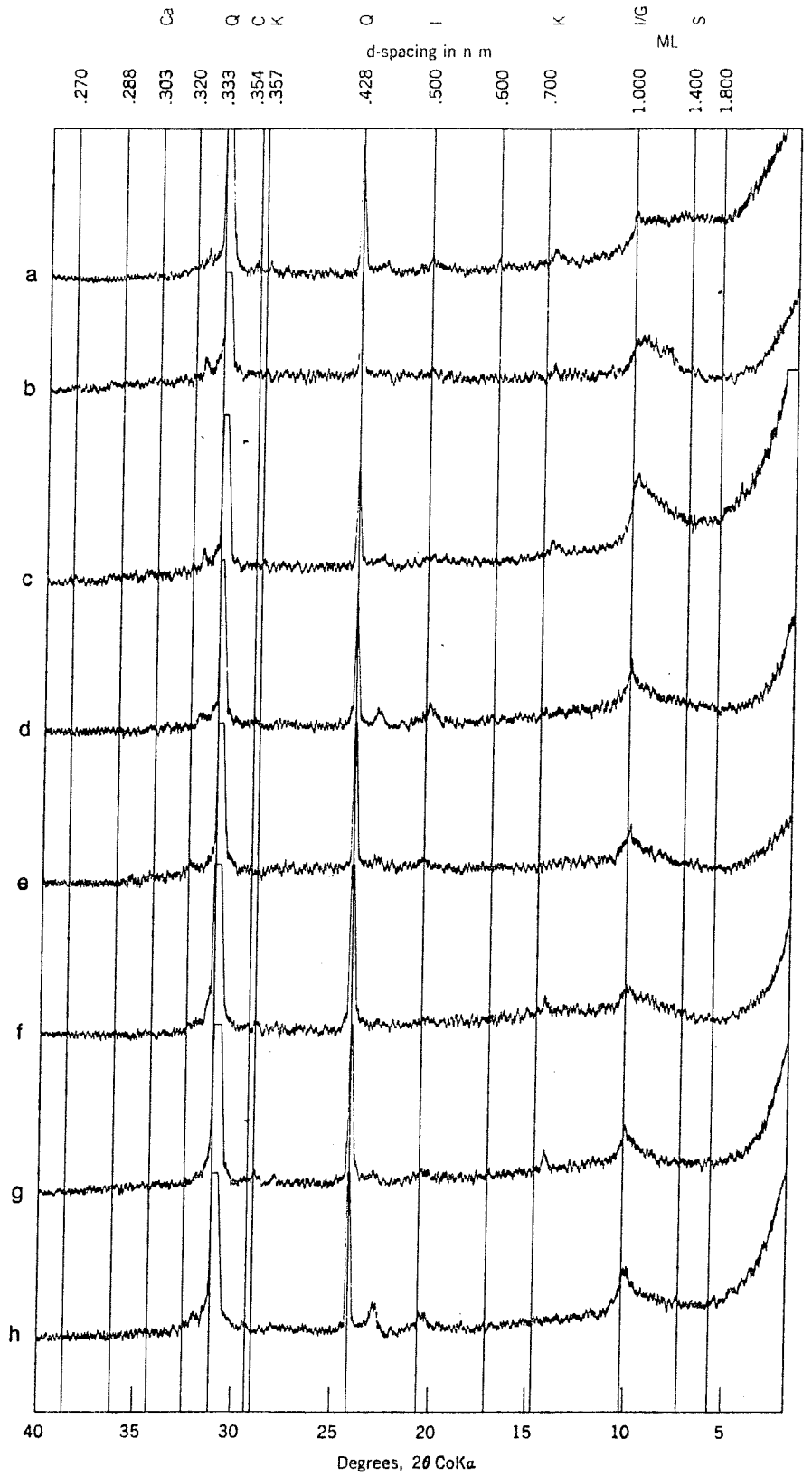

Figure 9. X-ray diffaction patterns of the <.2μm fraction from a calcareous sandstone, East Drake L-06 well,1128.91-1128.93 metres depth; (a) Ca-saturated, glycerol-treated specimen; (b) Ca-saturated specimen at 50 per cent R.H.; (c) Ca-saturated specimen at 0 per cent R.H.; (d) Ca-saturated specimen after heating at 550°C; (e) K-saturated, glycerol-treated specimen; (f) K-saturated specimen at 0 per cent R.H.; (h) K-saturated specimen after heating at 550°C.

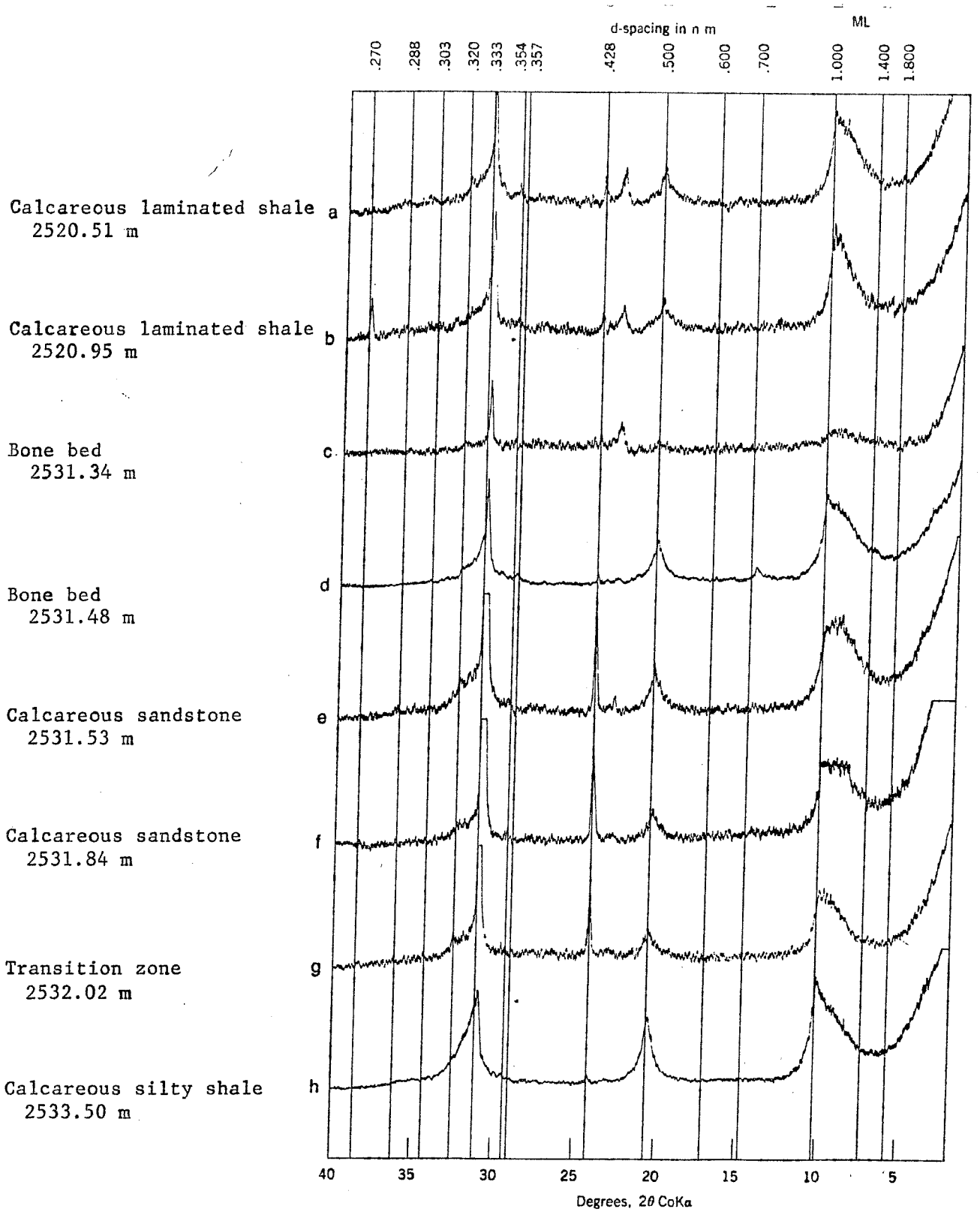

Figure 10. X-ray diffraction patterns of Ca-saturated <.2μm fraction from Skybattle Bay M-11 well samples, at 50 per cent R.H.; (a) Calcareous laminated shale at 2520.51 metres depth; (b) Calcareous laminated shale at 2520.95 metres depth; (c) Bone bed (major unconformity) AT 2531.34 metres depth; (d) Bone bed (major unconformity) at 2531.48 metres depth; (e) Bioturbated calcareous sandstone at 2531.53 metres depth; (f) Bioturbated calcareous sandstone from 2531.84 metres depth; (g) Transition zone at 2532.02 metres depth; (h) Calcareous silty shale at 2533.50 metres depth.

APPENDIX I

MODIFICATION OF STOKE'S LAW TO OBTAIN THE <.2μm FRACTION BY CENTRIFUGATION

Use of Stoke's law in Centrifugation to separate sizes

Stoke's in 1851 established a relationship between size and settling velocity for small spheres.

When a small sphere is placed in a viscous fluid with a density less than that of the sphere then the latter will begin and continue to fall under the influence of gravitation force, bouyant force of fluid and frictional resistance of fluid.

When the

Gravitational force = Bouyant force + Viscous resistance

then a terminal velocity will be reached. This velocity can be calculated as follows:

$$4/3 \times N \cdot R^3 P_S \cdot g = 4/3 \cdot n \cdot r^3 \cdot g + 6nr\eta v$$

However, if instead of gravitational force we apply the centrifugal force then:

$$4/3nr^3 P_S F_C = 4/3nr^3 p_L F_C + 6nr\eta v$$

$$4/3nr^3 F_C (P_S - P_L) = 6nr\eta v$$

since

$$F_C = \frac{V^2}{R} = \frac{(2nRN)^2}{R} = 4n^2 RN^2$$

then

$$4/3nr^3 \cdot 4n^2 RN^2 (P_S - P_L) = 6nr\eta v$$

or

$$v = \frac{4}{18} \times \frac{4n^2 r^3 N^2 R}{r\eta}(P_S - P_L) = \frac{8}{9}\frac{r^2}{\eta}(P_S - P_L) n^2 N^2 R$$

if

$$\frac{8}{9}\frac{n^2 N^2}{\eta}(P_S - P_L) = K$$

then

$$v = Kr^2 R$$

rearranging we obtain

$$\frac{dR}{R} = Kr^2 dt$$

Integrating between R_1 and R_2 (R_1 = distance in cm of the top of clay suspension from the rotational axis and R_2 = distance in cm at sedimented material, after centrifugation, from the rotational axis) and t_0 (time zero) and t_1, we obtain:

$$\frac{R_2}{R_1}\frac{dR}{R} = Kr^2 \frac{t_1}{t_2} dt$$

$$ln \frac{R_2}{R_1} = Kr^2(t_1 - t_0)$$

$$t_1 = \frac{1}{Kr^2} In \frac{R_2}{R_1}$$

more analytically

$$t_1 = \frac{9}{8} \frac{n}{n^2 N^2 (P_S - P_L)} \times 2.303 \, log_{10} \frac{R_2}{R_1} \times \frac{1}{r^2}$$

The symbols in the equations dealing with centrifugal force mean the following:

F_C = centrifugal force

V = rotational velocity of particle about centrifugal axes is cm/sec

R = distance of particle from axes of rotation in cm

R_1 = distance of top of clay suspension from axes of rotation in cm

R_2 = distance of sedimented material from axes of rotation in cm

v = particle velocity in the direction of R

N = number revolutions per second

t = time in sec

η = viscosity in poise (gm/sec/cm)

s = depth in cm

g = gravity acceleration (980 cm/sec2)

P_S = particle density

P_W = water density

r^2 = radii of particle in cm

Example:

For R_2 = 17 cm, R_1 = 12 cm, N = 2.500 R.P.M. (2.500/60 = 41 R.P.S.) therefore N = $(41)^2$.

$\eta = 8.9 \times 10^{-3}$, $P_S - P_L \simeq 1.2$ and d = 0.21 ($r = 10^{-1}\mu$ or 10^{-5} cm). What is the time required?

$$t = \frac{9}{8} \times \frac{8.9 \times 10^{-3}}{(3.14)^2} \times 2.303 \log \frac{21}{12} \times \frac{1}{(10^{-5})^2} = 2.81 \times 10^3 \text{ sec or } 46.9 \text{ min.}$$

For the international centrifuge, head #277, assuming 2800 R.P.M, we have:

N = revolutions/sec.

R_1 = radius to top of liquid (12.5 cm)

R_2 = radius to bottom of liquid (17.5 cm)

P_S-P_W = density of sample minus density of water = 1.20

7 = particle size in cm ($.2\mu = 1 \times 10^{-5}$)

n = viscosity in poise - at 25°C 8.9×10^{-5}

$$t = \frac{9}{8} \times \left(\frac{n}{\pi^2 N^2 (P_S - P_W)}\right) \times 2.303 \log_{10} \frac{R_2}{R_1} \times \frac{1}{r^2} = 24.67 \text{ min.}$$

Semi-quantitative analysis by X-ray diffraction on the <.2 μ fraction of East Drake L-06 well

Depth in metres	Illite	Kaolinite	Expandable and/or Mixed layer clays	Quartz	Lithology
1122.68-1122.71	+ +	+	+ +	tr	Brown shale
1122.76-1122.79	+ +	+	+ +	+	Brown shale
1122.86-1122.89	+ +	-	+ +	-	Brown shale
1123.38-1123.40	+ + +	-	tr	+ +	Green shale
1124.02-1124.04	+ +	-	+ + +	+	Green shale
1124.15-1124.18	+ +	-	+ + +	tr	Green shale
1124.53-1124.55	+ + +	-	+ +	+ +	Green shale
1125.12-1125.15	+ + +	-	+	+	Green shale
1125.92-1125.95	+		+ + +	+	Calcareous sandstone
1127.64-1127.66	+ +	-	+ +	+ + +	Calcareous sandstone
1128.91-1128.93		-	+	+ + +	Calcareous sandstone
1130.22-1130.25	+	tr	+ +	+ + +	Glauconitic sandstone
1130.93-1130.95	-	-	+	+ + + +	Glauconitic sandstone
1131.72-1131.74	-	+	+ +	+ + +	Glauconitic sandstone
1131.89-1131.91	+ +	+	+ +	+ +	Argillaceous siltstone
1132.26-1132.28	+ +	+ + +	+ +	+ +	Argillaceous siltstone
1132.65-1132.67	+ +	+ +	+	+ +	Sandy limestone
1133.57-1133.59	+	+	+ +	+ + +	Glauconitic sandstone
1134.83-1134.85	+ +	+ +	+ +	tr	Siltstone
1136.67-1136.70	+ +	+ +	+ +	+ +	Calcite
1136.70-1136.73	+	+	+	+ +	Glauconitic sandstone
1137.47-1137.49	+ +	+ +	+	+ +	Sandy limestone
1137.82-1137.84	+ + +	+ +	+ +	+ +	Brown calcareous shale
1138.50-1138.52	+ +	+ +	+	+	Brown calcareous shale
1139.06-1139.08	+ +	+ +	+	+	Brown calcareous shale
1140.03-1140.05	+	+ +	+	+ +	Brown calcareous shale
1141.03-1141.05	+ +	+ +	+ +	+ +	Brown calcareous shale
1141.15-1141.17	+ +	+ +	+ +	+ +	Brown calcareous shale
1141.34-1141.36	+	+	+ +	+ + +	Glauconitic sandstone
1141.87-1141.90	+ + +	+ + +	tr	+	Glauconitic sandstone
1143.73-1143.75	-	-	tr	+ + + +	Glauconitic sandstone
1144.10-1144.12	+	tr	+ +	+ + +	Sandy limestone
1144.49-1144.51	+ +	+ +	+ +	+ +	Sandy limestone
1146.08-1146.10	+ +	+ +	+	+ + +	Calcareous sandstone
1146.99-1147.01	-	tr*	tr	+ + + +	Sandstone
1147.54.1147.56	-	-	+	+ + + +	Sandstone
1148.06-1148.08	+	-	+ +	+ + +	Silty shale
1148.38-1148.40	-	**	+ +	+ + +	Silty shale
1148.76-1148.78	+	tr*	+	+ + +	Glauconitic sandstone
1149.57-1149.59	+ +	+ +	+ +	+ +	Limestone
1150.27-1150.29	-	-	+	+ + + +	Calcareous sandstone
1151.24-1151.26	+	+	+ +	+ + +	Calcareous sandstone
1151.63-1151.66	+	+	+ +	+ +	Calcareous sandstone
1151.94-1151.99	+	+*	+ +	+ + +	Calcareous sandstone
1152.66-1152.68	-	-	-	-	Calcareous sandstone
1153.14-1153.16	-	+*	+	+ + +	Calcareous sandstone
1154.01-1154.03	-	-	+	+ + + +	Calcareous sandstone
1154.38-1154.40	-	-	+	+ + + +	Calcareous sandstone
1155.05-1155.07	+	+*	+ +	+ + +	Calcareous sandstone
1157.42-1157.44	+	+*	tr	+ + +	Calcareous sandstone

**Amorphous hump
* Not well crystallized

TABLE 2

Semi-quantitative analysis by X-ray diffraction on the <.2 µm fraction of Skybattle Bay M-11 well

Depth in metres	Illite	Kaolinite	Expandable and/or Mixed layer clays	Quartz	Lithology
2520.02	-	-	+ +	+ +	Calcareous laminated shale
2520.51	+	-	+ + +	+	Calcareous laminated shale
2520.58	+ +	-	+ +	-	Calcareous laminated shale
2520.68	+ +	-	+ +	+	Calcareous laminated shale
2520.81	+ + +	-	+ + +	+	Calcareous laminated shale
2520.85	+ +	-	+ +	-	Calcareous laminated shale
2520.92	+ +	-	+ +	-	Calcareous laminated shale
2520.95	+ +	-	+	+	Calcareous laminated shale
2522.29	+ +	-	+ +	+	Calcareous laminated shale
2522.41	+ +	-	+ +	+	Calcareous laminated shale
2522.61	+ +	-	+ +	+	Calcareous laminated shale
2522.65	+ +	-	+ +	+	Calcareous laminated shale
2525.12	+ +	-	+ +	+	Calcareous laminated shale
2526.00	+ + +	-	+	+	Calcareous laminated shale
2527.08	-	-	+ + +	+	Calcareous laminated shale
2527.79	+ + +	tr	+	+	Calcareous laminated shale
2528.22	-	-	+ + +	+	Calcareous laminated shale
2528.54	-	-	+ + +	+	Calcareous laminated shale
2529.44	-	-	+ + +	+	Calcareous laminated shale
2530.04	-	-	+ + +	+	Calcareous laminated shale
2530.14	-	-	+ + +	+	Calcareous laminated shale
2530.24	-	-	+ + +	+	Calcareous laminated shale
2530.27	-	-	+ + +	+	Transition Zone
2531.16	-	-	+ + +	+	Bone bed, major unconformity
2531.25	-	-	+ + +	+	Bone bed, major unconformity
2531.34	-	-	+ +	+	Bone bed, major unconformity
2531.38	+ +	+	+ +	+	Bone bed, major unconformity
2531.44	+ +	-	+ +	+	Bone bed, major unconformity
2531.48	+ +	-	+ +	+	Bone bed, major unconformity
2531.53	+ +	-	+ +	+ +	Bioturbated calcareous sandstone
2531.84	+	-	+ +	+ +	Bioturbated calcareous sandstone
2531.93	+	-	+	+ + +	Bioturbated calcareous sandstone
2532.02	+ +	-	+ +	+	Transition Zone
2532.08	+ +	-	+ +	+	Calcareous silty shale or mudstone
2532.39	+ +	-	+ +	+	Calcareous silty shale or mudstone
2532.65	+ +	-	+ +	+	Calcareous silty shale or mudstone
2533.50	+ +	-	+ +	+	Calcareous silty shale or mudstone
2538.08	+ +	-	+ +	+	Calcareous silty shale or mudstone
2534.30	+ +	-	+ +	+	Calcareous silty shale or mudstone
2536.35	+ +	-	+ +	+	Calcareous silty shale or mudstone

TABLE 3

Thermogravimetric analysis of the air dried Ca-saturated <.2 µm fraction
Per cent absorbed, cavity, and crystal lattice H_2O on an air dry basis

Sample name	Absorbed H_2O ambient-250°C	Cavity H_2O 250-370°C	Crystal H_2O 370-1000°C	TOTAL LOI
East Drake L-06 Well				
1122.68-1122.71	6.00	2.60	9.00	17.60
1122.76-1122.79	3.30	1.40	6.20	10.90
1123.38-1123.40	3.90	0.90	5.30	10.10
1124.53-1124.55	3.40	0.90	6.50	10.80
1125.12-1125.18	4.80	0.80	5.20	10.80
1125.92-1125.95	5.90	0.70	5.00	11.60
1128.91-1128.93	1.00	1.90	5.90	8.80
1130.22-1130.25	1.60	1.30	4.70	7.60
1131.89-1131.91	3.10	0.60	5.10	8.80
1134.83-1134.84	3.10	1.30	8.20	12.60
1135.57-1135.59	0.50	0.60	2.10	3.20
1136.70-1136.73	2.70	0.60	5.70	9.00
1137.47-1137.49	2.20	1.80	5.00	9.00
1137.82-1137.84	2.00	0.70	6.10	8.80
1140.03-1140.05	2.60	0.90	8.60	12.10
1141.87-1141.90	0.60	0.50	3.20	4.30
1144.10-1144.12	0.80	1.00	2.60	4.40
1147.54-1147.56	0.50	0.40	1.50	2.40
1149.57-1149.59	1.90	0.70	5.40	8.00
1151.24-1151.26	1.40	0.60	3.20	5.20
1151.63-1151.66	1.50	0.40	3.30	5.20
1153.14-1153.16	0.60	0.60	1.90	3.10
1154.38-1154.40	0.60	0.50	2.50	3.60
Skybattle Bay M-11 Well				
2520.51	2.60	1.60	13.30	17.50
2520.95	3.10	1.70	14.50	19.30
2531.34	8.20	2.40	5.20	15.80
2531.38	2.50	1.10	7.50	11.10
2531.53	1.60	0.90	4.30	6.80
2531.84	1.50	0.90	4.60	7.00
2531.93	1.50	1.70	6.10	9.30
2533.50	3.00	0.80	6.20	10.00

TABLE 4

Thermogravimetric analysis of the Ca-saturated <.2 μm fraction after heating for 2 1/2 hours to 550°C. Per cent absorbed, cavity and crystal lattice H_2O on air dry basis

Sample Name	Absorbed H_2O ambient-250°C	Cavity H_2O 250-370°C	Crystal H_2O 370-1000°C	TOTAL LOI
East Drake L-06 Well				
1122.68-1122.71	6.20	2.80	3.60	12.60
1122.76-1122.79	2.10	2.80	4.20	9.1
1123.38-1123.40	1.90	1.30	2.50	5.70
1124.53-1124.55	3.00	1.10	3.10	7.20
1125.12-1125.18	2.50	1.80	3.10	7.40
1125.92-1125.95	3.60	1.10	3.60	8.30
1128.91-1128.93	1.00	0.90	2.50	4.40
1130.22-1130.25	0.90	0.90	2.80	4.60
1131.89-1131.91	1.50	0.50	1.90	3.90
1136.70-1136.73	1.50	0.50	1.90	3.90
1134.83-1134.84	2.50	0.80	3.10	6.40
1135.57-1135.59	0.50	0.30	0.90	1.70
1137.47-1137.49	1.50	0.40	2.00	3.90
1137.82-1137.84	-	-	-	-
1140.03-1140.05	2.20	1.30	3.10	6.60
1141.87-1141.90	6.00	3.50	6.60	16.10
1144.10-1144.12	1.30	0.50	1.30	3.10
1147.54-1147.56	1.60	0.40	0.90	2.90
1149.57-1149.59	1.20	0.40	1.90	3.50
1151.24-1151.26	1.10	0.70	1.40	3.20
1151.63-1151.66	1.00	0.40	1.50	2.90
1153.14-1153.16	0.40	0.30	0.50	1.20
1154.38-1154.40	0.50	0.15	0.75	1.40
Skybattle Bay M-11 Well				
2520.51	3.30	0.80	2.20	6.30
2520.95	1.70	0.70	2.80	7.20
2531.34	2.10	0.90	2.80	5.80
2531.38	1.50	0.40	2.30	4.20
2531.53	1.10	0.60	1.40	3.10
2531.84	0.90	0.30	1.80	3.00
2531.93	0.30	0.20	1.50	2.00
2533.50	2.10	0.50	4.40	7.00

TABLE 5

Absorbed and crystal-lattice water of clay minerals, and the temperature at the completion of desorption and at the start and completion of dehydration (after Barshead, 1965).

Clay Mineral	Absorbed water: Layer water %[1]	Absorbed water: Cavity water %[1]	Crystal-lattice water %[1]	Temperature at completion of desorption: Layer water °C	Temperature at completion of desorption: Layer water °C	Temperature at start of dehydroxlylation °C	Temperature at completion of dehydroxylation °C
Ca Montmorillonite	20.16	3.37	5.08	250	370	370	1,000
Na Montmorillonite[2]	14.00	0.00	5.05	150	-	150	1,000
Ca Vermiculite[2]	20.00	3.08	4.80	250	700	250	1,000
Na Vermiculite	10.14	4.66	4.76	150	700	150	1,000
Ca Illite[2]	5.16	1.06	4.97	150	370	370	1,000
Na Illite	3.45	0.66	5.07	150	370	370	1,000
Muscovite[2]	1.00	0.45	4.74	250	350	370	1,000
Phlogopite[2]	0.4-1.0		4.51	350		350	1,000
Biotite[2]	0.4-1.5		4.17	350		350	1,000
Talc[2]	0.7-1.0		4.99	350		350	1,000
Pyrophylite[2]	0.5-1.5		5.26	350		350	1,000
Kaolinite [3]	0.2-1.2		16.20	350		350	1,000
Halloysite (hydrated)	13.2		16.20	250		350	1,000
Chrysotile and antigorite	1.0-2.0		14.95	250		350	1,000
Clinochlore[4]	0.2-0.5		14.81	250		370	1,000
Ripidolite	0.2-0.5		13.39	250		370	1,000
Sheridinite	0.2-0.5		14.81	250		370	1,000
Gibbsite	0.5-0.6		52.95	100		150	350
Goethite	0.0-0.1		33.80	100		200	370
Brucite	0.5-0.6		44.70	170		200	370

[1]On the ignited basis
[2]:1 minerals
[3] 1:1 minerals
[4] 2.2 minerals

TABLE 6

Crystal lattice H_2O on ignition basis, semiquantitative concentration of 2:1 layer silicates, per centabsorbed and cavity H_2O on the 2:1 layer silicates

Depth in metres	Crystal lattice H_2O on ignition basis[1]	Semiquantitative** concentration of 2:1 layer silicates[2]	Per cent absorbed and cavity H_2O on air dry basis in the sample[3]	Per cent absorbed and cavity H_2O on air dry basis in the 2:1 layer silicates[4]
1122.68-1122.71	4.1	82	8.60	10.5
1122.76-1122.79	4.6	92	4.70	5.1
1123.38-1123.40	2.6	52	4.80	9.2
1124.53-1124.55	3.3	66	4.30	6.5
1125.12-1125.18	3.3	66	5.60	8.5
1125.92-1125.95	3.9	78	6.60	8.5
1128.91-1128.93	2.6	52	2.90	5.6
1130.22-1130.25	2.8	56	2.90	5.6

1 Crystal lattice H_2O for sample 1122.68-1122.71 metres depth is given on Table 4 as 3.6% on an air dry basis, therefore on an ignition basis it is: $100 \times 3.6 \div 100 - 12.6 = 4.12$ per cent.

2 Table 5 yields a crystal lattice water value of 4.97% and 5.0% of Ca-illite. This value approximates the crystal lattic water of the expandable 2:1 layer silicates. Therefore the concentration of layer silicates for the sample from 1122.68-1122.71 metres depth is computed as follows: $4.1 \times 100 \div 5.0 = 82\%$.

3 Values from Table 3.

4 Value of column 4 obtained from columns 2 and 3 as follows: $8.60 \times 100 \div 82 = 10.5$.

TABLE 7

Elemental analysis of <.2 µm fraction on air dry basis

Depth in metres	SiO_2	Al_2O_3	TiO_2	Fe_2O_3	CaO	MgO	Na_2O	K_2O	H_2O
East Drake L-06 Well									
1122.68-1122.71	45.7	22.6	1.0	4.8	0.7	1.9	1.4	4.3	17.6
1122.76-1122.79	49.4	24.9	1.0	4.1	1.1	2.0	1.8	4.8	10.9
1123.38-1123.40	50.8	24.9	1.0	4.6	0.1	3.1	1.1	6.7	10.7
1124.53-1124.55	50.7	24.8	1.0	5.0	0.1	2.7	1.0	4.4	10.8
1125.12-1125.18	60.3	17.9	0.7	2.8	0.1	2.3	0.2	4.6	10.8
1125.92-1125.95	58.2	18.2	1.0	2.8	0.7	2.5	0.2	5.2	11.6
1128.91-1128.93	80.4	7.2	N.D.	0.9	0.6	0.4	N.D.	2.0	8.8
1130.22-1130.24	80.6	7.5	N.D.	1.2	N.D.	0.5	N.D.	2.6	7.6
1131.89-1131.91	61.4	19.6	0.7	1.3	0.2	1.3	3.3	3.4	8.8
1132.65-1132.67	54.2	27.2	1.3	2.5	0.1	1.1	0.9	3.7	9.0
1134.83-1134.84	50.7	26.1	1.2	2.9	0.3	1.4	0.5	4.3	12.6
1136.70-1136.73	67.6	18.7	0.9	1.5	0.4	1.4	2.8	3.5	3.2
1137.47-1137.49	70.5	14.2	0.6	1.5	0.9	0.5	0.9	1.9	90.0
1137.82-1137.84	61.1	21.3	1.1	1.6	0.4	.2	1.0	4.5	8.8
1140.03-1140.05	52.4	26.9	0.8	2.5	0.2	1.1	0.8	3.2	12.10
1141.87-1141.90	57.2	26.1	0.7	3.7	tr	1.6	1.0	5.4	4.30
1144.10-1144.12	64.7	19.4	0.7	3.4	0.2	1.6	0.9	4.7	4.40
1147.54-1147.56	75.2	14.6	1.0	2.9	tr	1.0	tr	2.9	2.40
1149.57-1149.59	61.5	16.9	0.9	5.8	0.3	1.4	0.6	4.6	8.0
1151.24-1151.26	82.7	6.6	tr	2.7	tr	0.9	tr	1.9	5.2
1151.63-1151.66	82.4	7.4	tr	2.4	0.5	0.4	tr	1.7	5.2
1153.14-1153.16	80.1	10.2	0.3	2.4	tr	0.8	0.3	2.8	3.1
1154.38-1154.40	82.7	9.1	0.2	1.8	trs	0.6	0.24	2.3	3.6
Skybattle Bay M-11 Well									
2520.51	50.8	20.6	1.0	1.9	0.6	2.0	0.7	4.9	17.50
2520.95	48.8	19.4	1.4	2.8	0.7	1.9	0.7	5.0	19.30
2531.34	53.5	22.7	0.8	1.9	0.1	1.0	0.9	3.3	15.80
2531.38	73.1	9.9	0.7	1.2	0.1	0.6	0.3	3.0	11.10
2531.53	76.3	10.9	N.D.	2.3	N.D.	0.7	0.3	2.7	6.80
2531.84	71.1	13.7	0.6	2.7	0.1	0.9	0.7	3.2	7.00
2532.02	71.3	13.4	N.D.	2.7	0.1	0.6	N.D.	2.6	9.30
2533.50	62.9	17.3	1.0	3.0	0.1	1.0	0.3	4.4	10.00

TABLE 8

Per cent 2:1 layer silicates and K2O content in the < .2μm fraction, per cent K_2O content in the 2:1 layer silicates

Depth in metres	Lithology	Per cent 2:1 layer silicates in <.2μm fraction	Per cent K_2O in the <.2μm fraction	Per cent K_2O in the 2:1 layer silicates
East Drake L-06 well				
1122.68-1122.71	Brown shale	82	4.3	5.2
1122.76-1122.79	Brown shale	92	4.8	5.2
1123.38-1123.40	Green shale	52	3.7	7.1
1124.53-1124.55	Green shale	66	4.4	6.7
1125.12-1125.18	Green shale	66	4.6	7.0
1125.92-1125.95	Calcareous sandstone	78	5.2	6.7
1128.91-1128.93	Calcareous sandstone	52	2.0	3.8
1130.22-1130.25	Calcareous sandstone	56	2.0	3.6